Shock Wave Study on the Thermal Unimolecular Decomposition of Allyl Radicals

Ravi X. Fernandes, Binod Raj Giri, Horst Hippler,* Chatuna Kachiani, and Frank Striebel*

Institut für Physikalische Chemie, Lehrstuhl fur Molekulare Physikalische Chemie, Fritz Haber Weg 4, 76131 Karlsruhe, Germany

Received: June 11, 2004; In Final Form: November 9, 2004

We present the first direct study on the thermal unimolecular decomposition of allyl radicals. Experiments have been performed behind shock waves, and the experimental conditions covered temperatures ranging from 1125 K up to 1570 K and pressures between 0.25 and 4.5 bar. Allyl radicals have been generated by thermal decomposition of allyl iodide, and H-atom resonance absorption spectroscopy has been used to monitor the reaction progress. A marked pressure dependence of the rate constant has been observed which is in agreement with the results from a master equation analysis. However, our experimental results as well as our Rice−Ramsperger−Kassel−Marcus calculations seem to contradict the results of Deyerl et al. (*J. Chem. Phys.* **1999**, *110*, 1450) who investigated the unimolecular decomposition of allyl radicals upon photoexcitation and tried to deduce specific rate constants for the unimolecular dissociation in the electronic ground state. At pressures around 1 bar we extracted the following rate equation: $k(T) = 5.3 \times 10^{79}(T/K)^{-19.29}$ exp[(−398.9 kJ/mol)/RT] s^{-1}. The uncertainty of the rate constant calculated from this equation is estimated to be 30%.

Introduction

Resonantly stabilized unsaturated hydrocarbon radicals are thought to play a crucial role in the formation of aromatics, which eventually might lead to the formation of soot, in combustion processes. As a result of their relative high thermal stability and their slow reaction with molecular oxygen, these radicals can build up high concentrations in combustion systems under fuel-rich conditions. The simplest of these radicals are propargyl (C_3H_3) and allyl (C_3H_5) radicals. The role of propargyl and allyl for the formation of benzene has been discussed in the past (see, e.g., ref 1). However, to the best of our knowledge no direct study on any reaction involving allyl radicals has been performed under high-temperature conditions. This fact motivated us to investigate reactions of allyl radicals, and we decided to start with a study on the thermal unimolecular decomposition of this species.

So far only one indirect study on the thermal unimolecular decomposition of allyl radicals has been published. Tsang and Walker studied the pyrolysis of 1,7-octadiene (relative concentrations ranging from 30 to 1000 ppm) in the temperature range from 1040 to 1200 K and at pressures ranging from 2 to 7 atm doing shock tube experiments.[2] The pyrolysis was modeled with a mechanism containing 24 reactions, and rate constants of allyl radical reactions were adjusted to match the results of an end products analysis obtained from gas chromatography−mass spectrometry. At 1080 K, a rate constant of 40 s^{-1} has been extracted for the unimolecular decomposition of allyl radicals. Additionally, the authors of ref 2 did a master equation analysis of the allyl decomposition reaction to support their modeling and to extract thermodynamic data for allyl. At the time when ref 2 was published no information on the potential energy surface (PES) for the allyl decomposition was available, and, thus, the authors had to make some assumptions for their calculations. One assumption was that the only products of the decomposition are allene and H atoms. The authors extracted a high-pressure rate constant of $1.5 \times 10^{11}T^{0.84}$ exp(−30 053/T) s^{-1} and a step-size down parameter of 500 cm^{-1} for the collisional deactivation. Because the authors of ref 2 had to make some estimates on the rate constants needed for the mechanism, the extracted rate constant might be rather uncertain and, hence, a more direct determination of the rate constant seems to be desirable.

More recently, Deyerl et al. studied the unimolecular decomposition of allyl radicals upon photoexcitation at energies around 40 700 cm^{-1}.[3] They generated allyl radicals using a technique called supersonic jet flash pyrolysis and used H-atom photoionization with Lyman α radiation to monitor the reaction progress. From their experimentally observed H-atom time profiles they concluded that two reaction channels compete: one leading to allene plus H and a second one yielding 2-propenyl which decomposes further to yield H + propyne. The authors also determined specific rate constants [$k(E)$] which were found to be in reasonable agreement with their own Rice−Ramsperger−Kassel−Marcus (RRKM) calculations. However, they are not able to provide a sound justification for the analysis of their experimental results. In particular, they fail to provide a mechanism which is capable of reproducing the experimentally observed H-atom time profiles. Specific rate constants and thermal rate constants [$k(T, p)$] are, of course, closely related to each other, and, therefore, we should take into account the results from ref 3 when discussing our experimental data.

The goal of the present study is to carry out a direct study on the pressure and temperature dependence of the rate constant for the allyl decomposition for the first time. We will also present a master equation analysis which helps to identify the initial pathways in the thermal unimolecular decomposition.

Experimental Section

The experiments were performed behind shock waves in a stainless steel shock tube, which is suited for experiments up to 10 bar. Because the setup has been described previously[4] we will give only a brief summary. The high-pressure section of the tube is 3.05-m long and has an inner diameter of 9.85 cm.

* Authors for correspondence. E-mail: horst.hippler@chemie.uni-karlsruhe.de (H.H.); frank.striebel@chemie.uni-karlsruhe.de (F.S.).

10.1021/jp047482b CCC: $30.25
Published on Web 01/20/2005

In contrast, the inner diameter of the low-pressure section is 10 cm, and this section is 4.20-m long. The two sections are separated by an aluminum foil, whose thickness is varied between 40 and 100 μm depending upon the pressure and temperature one wants to obtain behind the shock wave. To generate the shock waves hydrogen (Messer-Griesheim, >99.8%) is driven in the high-pressure section until the foil bursts. The driven gas is essentially argon (Messer-Griesheim, >99.9999%) containing only a small fraction (≤10 ppm) of the radical precursor allyl iodide (97%; Lancaster). Because we used such low mole fractions of the radical precursor we could calculate the post-shock conditions treating the test gas as pure argon. Furthermore, the calculations are based on the one-dimensional conservation equations and require the pre-shock conditions (T and p) as well as the speed of the shock wave, which was measured using four pressure transducers, as input parameters. We measured the speed of the shock wave at three positions and could, therefore, check if damping of the shock wave had to be taken into account for the calculations. For the low-pressure experiments a Laval nozzle was inserted in the low-pressure region directly behind the membrane separating the low- and the high-pressure parts to attenuate the shock.

We observed the decomposition of allyl radicals using time-resolved H-atom resonance absorption spectroscopy (H-ARAS) at 121.6 nm (Lyman α line). The Lyman α radiation is produced by a microwave discharge lamp consisting of a microwave generator (Muegge), a resonator, and a quartz tube. The microwave generator produces radiation at 2450 MHz with a typical power of 100 W. The resonator is mounted to the quartz tube, and a He mixture containing ~1% H_2 is flown through this tube at a pressure of 7 mbar. One end of the tube is connected to the shock tube and the vacuum ultraviolet (VUV) light transmits through the shock tube via MgF_2 windows. To detect Lyman α radiation we use a VUV monochromator (Acton Research Corp., Spectra Pro VM-504), which is connected to the shock tube and which is operated at pressures below 10^{-5} mbar, to spectrally isolate this line, and a solar blind photomultiplier (Hamamatsu, R1259). The signal from the multiplier is stored on a digital oscilloscope (Tektronix, TDS 540 A). With our current experimental setup we can detect H-atom concentrations between 5×10^{-13} and 1×10^{-10} mol/cm^3. The lower and the upper detection limits are due to noise of the detection system and to saturation of the optical transition, respectively.

Prior to each experiment the shock tube was evacuated to pressures below 5×10^{-7} mbar. The cleanliness of the shock tube as well as the gas mixing and inlet system was checked regularly by performing experiments in pure argon at temperatures around 2000 K. In cases where an absorption signal at 121.6 nm was observed in these experiments, which is only seldom the case, we cleaned the tube by performing a few shots with argon or mechanically.

The test gas mixtures and mixtures for calibration of the ARAS signal were prepared in two different mixing vessels made of stainless steel and having a volume of 100 l. These vessels were evacuated below 10^{-7} mbar before the mixtures were prepared, and the mixtures were allowed to homogenize for at least 12 h. Allyl iodide was degassed by several pump−freeze cycles prior to use, and all other gases were used without further purification. The test gas mixtures contained 2.8−10.2 ppm allyl iodide in argon, and the calibration mixtures contained 100−150 ppm N_2O (99%; Messer-Griesheim) and 1000−1570 ppm H_2 diluted in argon. Experiments were performed at pressures from 0.25 to 4 bar and temperatures between 1150 and 1500 K.

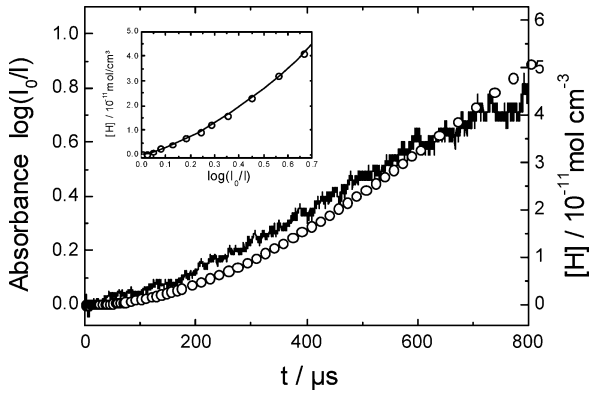

Figure 1. Typical result for a calibration of the H-ARAS detection system. Solid line, absorbance-time profile; dots, modeled H-atom time profiles. The mechanism used for the modeling is given in Table 1; for further discussion, see text. Experimental conditions for the calibration experiment: $T = 1350$ K and $p = 4.2$ bar. In the inset the corresponding calibration curve is depicted.

TABLE 1: Mechanism Used To Model the H-Atom Concentration-Time Profiles in the Calibration Experiments[a]

reactants		products	n	log(A)	E_a, kJ/mol	ref
$N_2O + M$	⇒	$N_2 + O + M$		14.6	237	25
$O + H_2$	⇒	$OH + H$	2.7	4.7	26	26
$OH + H_2$	⇒	$H_2O + H$	1.6	8	14	26
$N_2O + H$	⇒	$N_2 + OH$		14.3	70	27
$N_2O + O$	⇒	$N_2 + O_2$		14	117	28
$H + OH + M$	⇒	$H_2O + M$	−2	21.9		26
$O + O + M$	⇒	$O_2 + M$	−1	17		29
$OH + OH$	⇒	$H_2O + O$	1.2	8.8		30
$OH + O$	⇒	$H + O_2$		13.2	3	26
$H_2 + M$	⇒	$H + H + M$	−1.1	18.8	437	31
$H + H + M$	⇒	$H_2 + M$	−1	17.8		31

[a] $k(T) = AT^n \exp\{-E_a/(RT)\}$.

Results

To extract the rate coefficients from experimentally observed absorbance-time profiles we first have to convert the absorbance in absolute H-atom concentrations. As a result of the spectral characteristics of the ARAS lamp—self-absorption and self-reversal lead to a poorly characterized profile of the emission line which is also broader then the absorption line of the H atoms to be detected—we cannot apply the Beer Lambert law to do this conversion. Instead we have to do calibration experiments in which we produce a known concentration of H atoms and calibrate the absorbance. Because this calibration should be done under conditions (T, p) similar to those of the actual experiment we employ the well-known N_2O/H_2 system for this.[5,6] When heated behind shock waves N_2O decomposes fast to produce O atoms which then react further with H_2 to yield OH + H. The consecutive reactions are well-characterized so that the H-atom concentration-time profiles in these experiments can be accurately modeled. By comparison between the modeled H-atom concentration-time profile and the observed absorbance-time profile calibration curves for the optical detection system are obtained. In Figure 1 we present the result of such a calibration curve, and in Table 1 we present the mechanism used for the calibration. At this point we want to stress that the extracted rate constants critically depend on the calibration, and we have the experience that the calibration depends on a number of parameters such as temperature and pressure as well as the "performance" of the lamp. We, thus, decided to do calibration experiments after every third experiment to minimize uncertainties in the rate constant due to

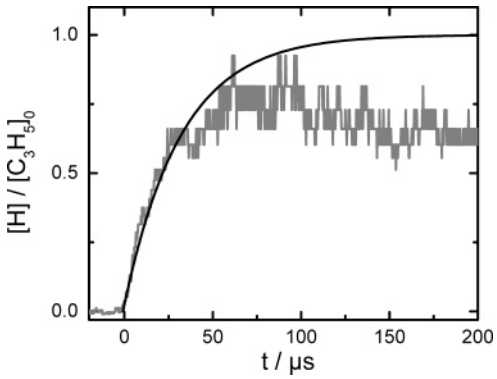

Figure 2. Typical experimental result. Grey line, experimentally determined time profile of the H-atom concentration; black line, H-atom concentration-time profile as expected for a pure unimolecular decomposition.

uncertainties in the calibration. From our experience we learned that this procedure leads to more reliable results although it is of course much more time consuming than using a single calibration curve for all experiments. The calibration experiments have been performed at pressures from 0.3 to 4.5 bar and temperatures between 1250 and 1700 K. As observed earlier we found the calibration curves to be pressure-dependent but only weakly temperature-dependent.[7]

The rate coefficients for the unimolecular decomposition of allyl radicals have been determined from the initial slope of the H-atom time profiles making use of the following relation:

$$\left(\frac{\mathrm{d}[H]}{\mathrm{d}t}\right)_{t=0} = k[\mathrm{C_3H_5}]_0 \qquad (1)$$

We assumed that the only products of the allyl iodide decomposition are allyl and iodide and, thus, that the initial allyl concentration is equal to the concentration of the radical precursor employed in the experiment.

A typical experimentally observed H-atom time profile is shown in Figure 2. As a result of low concentrations of the radical precursor we can eliminate competing bimolecular reactions at early times and, thus, use eq 1 for the data evaluation. We also checked if those competing reactions can be neglected by changing the concentration of the precursor and, thus, changing the rate of the bimolecular reactions. No dependence of the extracted unimolecular rate constant by use of eq 1 on the precursor concentrations was observed. At later times the observed H-atom time profile deviates from a single-exponential rise as a result of the fact that the unimolecular rate decreases and that the bimolecular reaction can compete. A simple mechanism consisting of 10 reactions was used to model the complete H-atom time profile. This mechanism will be discussed in the next section. All experimental results as well as conditions are summarized in Table 2.

TABLE 2: Summary of the Experimental Results

$x(C_3H_5I)$, ppm	T_5, K	p_5, mbar	[Ar], 10^{-5} mol/cm^3	[C_3H_5I], 10^{-11} mol/cm^3	k_{exp}, s^{-1}
2.8	1176	4354	4.45	12.1	695
2.8	1180	4297	4.38	11.9	1206
3.8	1313	4208	3.86	39.3	7900
3.8	1249	377	0.363	1.36	565
3.8	1278	326	0.307	1.15	784
3.8	1344	330	0.295	1.11	2207
4.8	1282	4526	4.26	20.1	5273
4.8	1237	4331	4.21	20.0	1873
4.8	1123	4462	4.78	23.4	221
4.8	1477	1248	1.02	4.82	27 912
4.8	1313	1248	1.14	5.42	3505
4.8	1308	1309	1.2	5.71	3345
4.8	1245	1287	1.24	5.89	924
4.8	1158	1235	1.28	6.08	141
9.8	1270	4318	4.09	40	4582
9.8	1241	4225	4.09	40.1	2042
9.8	1191	4485	4.53	44.3	1060
9.8	1158	4337	4.51	44	677
9.8	1567	300	0.23	2.25	19 417
9.8	1543	337	0.263	2.57	14 977
9.8	1472	354	0.289	2.83	9551
9.8	1304	337	0.311	3.04	1147
9.8	1282	361	0.338	3.30	1014
9.8	1194	360	0.362	3.54	168
9.8	1401	1267	1.09	10.6	12 491
9.8	1349	1226	1.09	10.7	5898
9.8	1274	1301	1.23	12.0	2100
9.8	1210	1286	1.28	12.5	644
9.8	1176	1270	1.30	12.7	260
10.2	1253	4498	4.32	43.8	3018
10.2	1237	4310	4.19	42.5	2508
10.2	1221	4427	4.36	44.5	2353
10.2	1210	4562	4.54	46	1543
10.2	1206	4340	4.33	43.9	1899
10.2	1126	4239	4.53	46	289
10.2	1561	295	0.227	2.32	17 845
10.2	1420	322	0.273	2.78	9238
10.2	1401	277	0.238	2.43	6008
10.2	1386	297	0.258	2.63	4061
10.2	1362	316	0.279	2.84	3007

Discussion

We start the discussion with a consideration about what reaction(s) yield the H atoms we are monitoring. Intuitively, one might write down the following possible reaction channels:

$$\mathrm{CH_2CHC^{\bullet}H_2} \rightarrow \mathrm{CH_2CCH_2} + \mathrm{H} \qquad (R1)$$

$$\mathrm{CH_2CHCH_2} \rightarrow \mathrm{CH_3CHC^{\bullet}H} \qquad (R2)$$

$$\mathrm{CH_2CHC^{\bullet}H_2} \rightarrow \mathrm{CH_3C^{\bullet}CH_2} \qquad (R3)$$

The propenyl radicals formed in reactions R2 and R3 might react further to yield H + propyne or allene.

While Tsang and Walker assumed that only reaction R1 occurs,[2] Deyerl et al. concluded from their experimental observations that both reaction R1 and reaction R3 occur upon photoexcitation with UV photons.[3] From our experimental observations we are not able to deduce unambiguously which reaction we are monitoring. Thus, we have to consult theoretical studies to get some insight in the mechanism of the reaction under investigation and we rely on the results from Davis et al.[8] The authors of ref 8 characterized the C_3H_5 PES using density functional theory (DFT) as well as ab inito methods (G2 calculations based on the DFT geometries and frequencies). To simplify the discussion we present in Figure 3 a sketch of the PES based on the results of ref 8. As is seen in Figure 3 the reaction R1 is energetically favored compared to R2 and R3 by roughly 3.5 kcal/mol. Note that Deyerl et al.[3] as well did some ab initio calculations, and their results agree qualitatively well with the results of ref 8: the differences between the results of ref 3 and ref 8 for the absolute values of the threshold energies for the competing reaction channels are a few kilocalories/mole. However, both studies predict that the threshold energies for R2 and R3 are ~3.5 kcal/mol above the one for R1. Because R1 is also entropically favored versus R2 and R3—the transition states for the latter reactions are much tighter than the one for R1—one would expect that R2 and R3 are of negligible

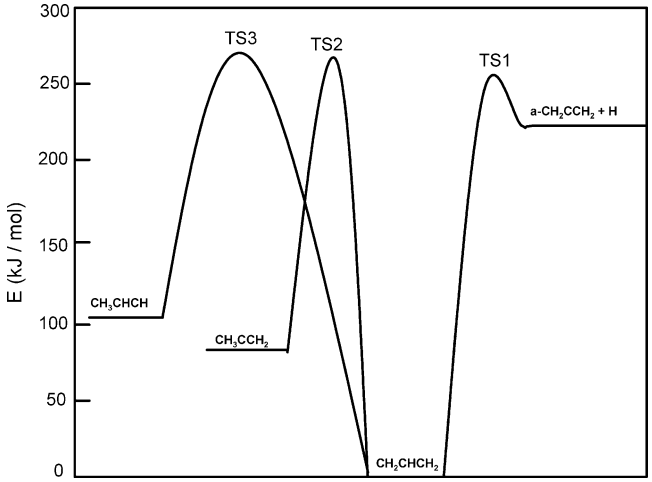

Figure 3. Sketch of the PES based on the results of ref 8. TS1, TS2, and TS3 correspond to R1, R2, and R3, respectively.

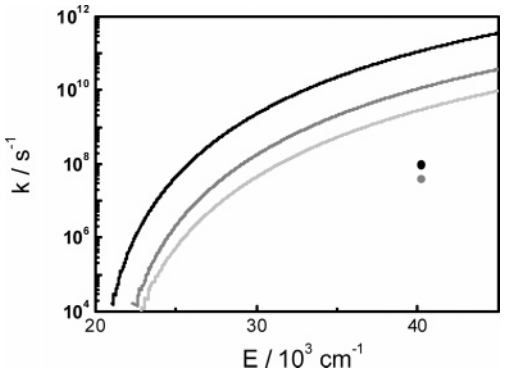

Figure 4. Specific rate constants as a function of energy. Black line, R1; gray line, R2; light gray line, R3; black symbol, rate constant given in ref 3 for R1; gray symbol, rate constant given in ref 3 for R2.

importance. This is best seen if one looks at the specific rate constants for the competing reaction channels, and in Figure 4 we present the results of a RRKM calculation. (The parameters used for the calculations are given in the appendix.) At all energies the rate constant for R1 is at least a factor of 20 higher than the ones for R2 and R3, and, thus, our calculations predict that allyl decomposes forming almost exclusively (≥95%) allene and H. This prediction is contradictory to the RRKM calculations of Deyerl et al.[3] as well as their extracted unimolecular rate constants, which both predict allene yields of about 70%. Note that the absolute values of the specific rate constants from ref 3 do not agree as well with our calculated RRKM results. We cannot comment on the RRKM calculations because the frequencies used for the calculations are not given in ref 3. However, it seems quite surprising that a channel having a higher threshold energy (∼3.5 kcal/mol) and proceeding via a highly strained transition state is only by a factor of ∼2 slower than the C−H scission.

The difference between our calculated rate constant and the specific rate constant extracted from experimental observations in ref 3 is about 3 orders of magnitude. This difference might be partly due to uncertainties in our calculations arising from uncertainties in the input parameters as well as from the simplified treatment neglecting anharmonic effects. However, we do not see any evidence from our master equation calculation that the RRKM calculations are entirely wrong (see below). One might try to match the experimental results from Deyerl et al. by increasing the density of states. We did this in several ways (lowering the three smallest frequencies and applying correction factors for the density of states) and calculated strong collision thermal rate constants. In any case these calculated rate constants were predicted to be almost pressure independent, which is not in agreement with our observations, and the absolute values for the strong collision rate constants were found to be at least 1 order of magnitude below our experimental results. We, thus, conclude that the specific rate constants from ref 3 are in agreement neither with our calculated RRKM results nor with our experimental observations. It is interesting to note that similar findings have been observed in the case of the ethyl decomposition: while a standard RRKM/master equation treatment is able to reproduce the observed pressure dependence of the thermal rate constant for this reaction[9,10] the specific rate constants found by the Chen group (using the same experimental approach as for the allyl radical) are 5 orders of magnitude smaller than the one predicted by RRKM theory.[11] The reason for these discrepancies between the experimental data from the Chen group and the RRKM calculations is at present not clear. However, from the results of the RRKM calculations one might expect that the time resolution used in the experiments from the Chen group is too low to monitor the dissociation on the ground state PES. The most probable explanation for the discrepancies seems to be that the dissociation from an excited state was observed in the experiments of refs 3 and 11 and that the photochemistry of these small hydrocarbon radicals is not entirely understood. Note that this explanation is in agreement with the finding of Zierhut et al. who extended their earlier experimental studies on the photodissociation of small hydrocarbon radicals[3,11] to the *tert*-butyl radical[12] and observe that the specific rate constants apparently decrease drastically at excitation energies around 30 500 cm^{-1}.

For the master equation treatment we assume that our calculated specific rate constants are of sufficient accuracy. For simplicity, we treat the reaction as one channel reaction assuming that allene and H atoms are the only products. This simplification leads to an underestimation of the thermal rate constants. However, the calculated specific rate constants indicate that the error due to this assumption is below 10% and, thus, well below the uncertainties of the calculations as well as the experiments. Within this model the high-pressure limiting rate constant was calculated to be

$$k_\infty(T) = 1.5 \times 10^{15} \exp\left(-\frac{265.6\ \text{kJ/mol}}{RT}\right) \text{s}^{-1} \qquad (2)$$

We will not discuss the master equation computations in detail because the procedure has been described in the literature (see, e.g., refs 7 and 13). For the analysis an exponential down model was used to treat the energy transfer process. The J dependence of the specific rate constants was neglected, and all calculations were performed with $k(E, J = 0)$. The analysis was done in two ways: one assuming a temperature-independent value for the energy transfer parameter α, which is approximately the mean energy transferred per downward collision ($\langle\Delta E\rangle_{\text{down}}$), and a second one assuming a temperature-independent value for the mean energy transferred per collision ($\langle\Delta E\rangle_{\text{all}}$). From the analysis we extracted values of $\alpha = 320\ \text{cm}^{-1}$ in the first case and $-\langle\Delta E\rangle_{\text{all}} = 85\ \text{cm}^{-1}$ in the second one. Only small differences (below a few percent) between the calculated rate constants were observed for the two approaches in the temperature and pressure range of our experiments. The absolute values of the energy transfer parameters are in accordance with results of master equation analysis for similar reactions (see, e.g., ref 14).

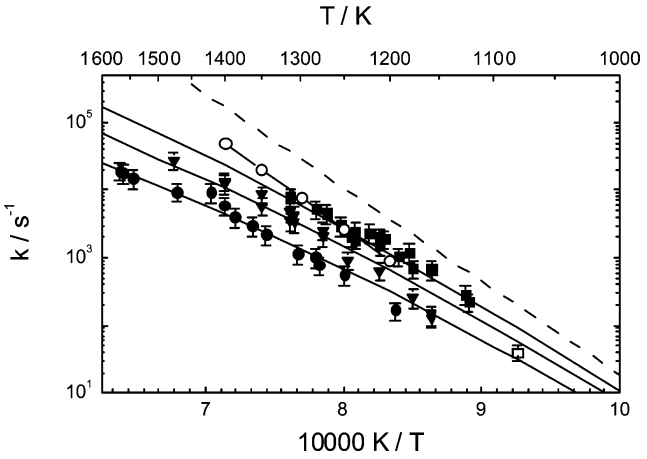

Figure 5. Arrhenius plot of the rate constants for R1. Solid symbols: experimental results for $p \sim 4$ bar (squares), ~1 bar (triangles), and ~0.25 bar (circles). The dotted line is the calculated high-pressure rate constant, and the solid lines are the calculated rate constants for p = 4, 1, and 0.25 bar (from top to bottom). The open square is the rate constant given in ref 2 for $p \sim 4$ bar, and the open circles are the results from the Troe group[15] obtained at pressures around 4.5 bar.

In Figure 5 we compare our experimental results with the results from the master equation calculations: the experimentally observed pressure and temperature dependence is nicely reproduced by the calculations. We also observe a fairly good agreement between our calculations and the result from Tsang and Walker.[2] As mentioned before, the authors of ref 2 also did a master equation analysis. Because details of the PES were not known at that time, they assumed $\langle \Delta E \rangle_{\text{down}}$ to be 500 cm^{-1} and fitted the high-pressure limiting rate constant. Because the chosen energy transfer parameter is too high, their extracted high-pressure limit is roughly 5 times smaller than the one we calculated. Also added in Figure 5 are unpublished results from the Troe group which were obtained at pressures around 4.5 bar using the shock tube technique and UV−absorption spectroscopy to detect allyl radicals.[15] The results of this work seem to support our experimental results. The fact that we observe good agreement between the experimental results and the calculation confirms our earlier assumption that the RRKM calculations are of sufficient accuracy.

From the results of our master equation computations we extracted the following modified Arrhenius expressions to describe the temperature dependence of the thermal rate constants in Ar:

$p = 0.25$ bar

$$k(T) = 4.7 \times 10^{81} \left(\frac{T}{K}\right)^{-20.07} \exp\left(-\frac{396.2\ \text{kJ/mol}}{RT}\right) \text{s}^{-1} \quad (3)$$

$p = 1$ bar

$$k(T) = 5.3 \times 10^{79} \left(\frac{T}{K}\right)^{-19.29} \exp\left(-\frac{398.9\ \text{kJ/mol}}{RT}\right) \text{s}^{-1} \quad (4)$$

$p = 4$ bar

$$k(T) = 6.2 \times 10^{79} \left(\frac{T}{K}\right)^{-19.10} \exp\left(-\frac{408.1\ \text{kJ/mol}}{RT}\right) \text{s}^{-1} \quad (5)$$

The uncertainties of the rate constants calculated from eqs 2−4 are estimated to be 30% in the temperature range from 1000 to 1600 K.

We also did some calculations for N_2 as the bath gas to provide more reliable data for combustion modeling. For this purpose, we set the energy transfer parameter $\alpha = 430$ cm^{-1}. This value was chosen on the basis of the energy transfer partner given in ref 14 for similar reactions: we assumed that the ratio of $\alpha(N_2)/\alpha(Ar)$ is the same for the reactions treated in ref 14 and the allyl decomposition, and we calculated $\alpha(N_2)$ from the energy transfer parameter extracted in the work for Ar as the collider. On the basis of this assumption we obtain the following expressions to describe the temperature dependence of the rate constant at different pressures:

$p = 0.25$ bar

$$k(T) = 1.8 \times 10^{69} \left(\frac{T}{K}\right)^{-16.43} \exp\left(-\frac{366.8\ \text{kJ/mol}}{RT}\right) \text{s}^{-1} \quad (6)$$

$p = 1$ bar

$$k(T) = 1.3 \times 10^{67} \left(\frac{T}{K}\right)^{-15.61} \exp\left(-\frac{369.1\ \text{kJ/mol}}{RT}\right) \text{s}^{-1} \quad (7)$$

$p = 4$ bar

$$k(T) = 6.8 \times 10^{64} \left(\frac{T}{K}\right)^{-14.75} \exp\left(-\frac{372.2\ \text{kJ/mol}}{RT}\right) \text{s}^{-1} \quad (8)$$

It should be mentioned that the differences between the calculated rate constants for N_2 as the bath gas and the one obtained in argon are small. This is expected because the rate constants are in the fall-off range. We recommend the rate constants calculated from eqs 6−8 for combustion modeling and estimate the uncertainties of the rate constants to be 30%.

So far we have only analyzed the observed H-atom time profiles at early times to extract rate coefficients for the decomposition of allyl radicals. As mentioned earlier we observed at longer times that the H-atom time profiles deviate from a single-exponential rise due to consecutive reactions in which H atoms are consumed. As a result of conditions existing in our experiments—low concentrations of all species except for that of the bath gas Ar—only few bimolecular reactions are likely to occur on the time scale of the experiments. Consequently, it is relatively simple to construct a mechanism for the reaction system and one might try to construct a mechanism and to model the experimental observations. A comparison between the experimental results and the predictions based on the model yields some insight into the validity of the model and also into the quality of the rate constants used for the modeling. Thus, the modeling of the H-atom time profiles might be used to check the accuracy of rate constants available in the literature, and it might be helpful to identify reactions for which further studies seem desirable. To avoid complications due to pressure-dependent rate constants we limit this modeling on experiments which have been performed at pressures around 1 bar.

Our model includes only nine reactions in addition to the allyl decomposition reaction: First we have to take into account that the allene formed in R1 isomerizes fast to yield propyne. This isomerization might either occur directly (H-atom shift) or by H-atom catalysis (H-atom addition followed by a fast C−H bond scission). Thus, we have to consider the following four reactions for our model:

$$CH_2CCH_2 \rightarrow CH_3CCH \quad \text{(R4)}$$

$$CH_3CCH \rightarrow CH_2CCH_2 \quad \text{(R5)}$$

$$CH_2CCH_2 + H \rightarrow CH_3CCH_2^* \rightarrow CH_3CCH + H \quad \text{(R6)}$$

$$CH_3CCH + H \rightarrow CH_3CCH_2^* \rightarrow CH_2CCH_2 + H \quad \text{(R7)}$$

Note that the chemically activated propenyl radicals formed in R6 and R7 are not thermally stable under the conditions of our experiments. Consequently, the stabilization of these radicals has not been taken into account. Whether R4 and R5 or R6 and R7 are the main pathway for the isomerization depends on the conditions of the experiment.

Next we have to think about which reactions H atoms might undergo: At the lowest temperatures H atoms are consumed by reactions which have low barriers. Those reactions are the combination of H atoms with allyl

$$CH_2CHCH_2 + H \rightarrow \text{products} \qquad \text{(R8)}$$

as well as addition reactions of H atoms to a double or a triple bond. Addition of H atoms to the central C atom (C2) of allene yields allyl.

$$CH_2CCH_2 + H \rightarrow CH_2CHCH_2 \qquad \text{(R9)}$$

Reactions R8 and R9 are most important at the lower temperatures at which allyl decomposes slowly. Additionally, we have to consider the H-atom addition to the central C atom of propyne forming chemically activated CH_3CHCH which decomposes fast to form acetylene and methyl radicals:

$$CH_3CCH + H \rightarrow CH_3CHCH^* \rightarrow CH_3 + C_2H_2 \qquad \text{(R10)}$$

At high temperatures H-atom abstraction reactions become competitive and we have to add the following two reactions to our mechanism:

$$CH_2CCH_2 + H \rightarrow CH_2CCH + H_2 \qquad \text{(R11)}$$

$$CH_3CCH + H \rightarrow CH_2CCH + H_2 \qquad \text{(R12)}$$

For the modeling we started with adopting rate constants from the literature. This led to an over-estimation of the H-atom time profiles at late reaction times and in particular at higher temperatures. The most sensitive reactions for the H-atom consumption are the reactions R8 and R10. At higher temperatures R11 and R12 might become important. For R8 no experimental data are available for high-temperature conditions. Thus, we relied on the result of a computational study[16] in which high-pressure rate constants are predicted. Consequently, the rate constant used has to be regarded as an upper limit. Additionally, this rate constant is expected to show a weak temperature dependence and, thus, is unlikely to be responsible for the observed discrepancies between experiments and the modeling. Because of those two reasons we did not adjust this rate constant to obtain a better agreement between our experimental observations and the results of the modeling.

For the reactions of H-atoms with propyne no experimental studies have been published. Therefore, we again relied on a computational study[17] in which stationary points of the PES for the H + propyne reaction have been characterized. The authors also calculated rate constants for the competing reaction channels as a function of pressure and temperature and found that the channel leading to CH_3 and C_2H_2 is dominant under the conditions of our experiment. We varied the rate constant given in ref 17 for reaction R10 within the typical uncertainties (at least a factor of 3) for these calculations. Additionally, we assumed that the rate constants for reactions R11 and R12 are identical. This assumption seems to be reasonable because the thermochemistry for both reactions is almost identical and because in both cases the same products are formed. The rate constant for R10 extracted in this way is given in Table 3 together with all other rate constants used. The agreement between our experimental observation and the mechanism listed in Table 3 is quite satisfying (see Figure 6). Consequently, we did not try to change any other rate constant. We want to stress that the same model was successfully applied in the modeling of shock tube experiments on the propyne as well as on the propargyl decomposition.[18]

TABLE 3: Mechanism Used To Model the Experimentally Observed H-Atom Concentration-Time Profiles at Pressures around 1.2 bar[a]

reaction	reactants		products	n	log(A)	E_a, kJ/mol	ref
R1	C_3H_5	⟹	a-C_3H_4 + H	−15.1	65	357.8	this work (see text)
R4	a-C_3H_4	⟹	p-C_3H_4	−7.80	39.90	328	32
R5	p-C_3H_4	⟹	a-C_3H_4	−13.9	60.70	381	32
R6	a-C_3H_4 + H	⟹	p-C_3H_4 + H	−0.91	17.79	42.2	8
R7	p-C_3H_4 + H	⟹	a-C_3H_4 + H	−0.91	17.79	42.2	8
R8	C_3H_5+ H	⟹	products	0.23	13.36	0.2	16
R9	a-C_3H_4 + H	⟹	C_3H_5		12.92	8.3	22
R10	p-C_3H_4 + H	⟹	C_2H_2 + CH_3		13.41	8.0	this work (see text)
R11	a-C_3H_4 + H	⟹	C_3H_3+ H_2	−1.75	8.54	31.84	17
R12	p-C_3H_4 + H	⟹	C_3H_3+ H_2	−1.75	8.54	31.84	17

[a] $k(T) = AT^n \exp\{-E_a/(RT)\}$.

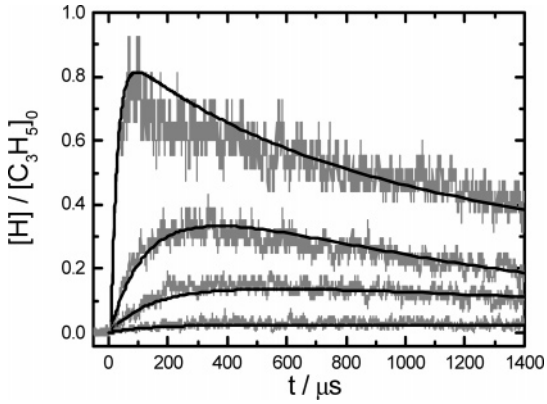

Figure 6. H-atom yields in the decomposition of allyl radical at different temperatures and at similar pressures. Experimental conditions (from top to bottom): $x_{(\text{allyl iodide})} = 4.8$ ppm, $T = 1477$ K, $p = 1.2$ bar; $x_{(\text{allyl iodide})} = 4.8$ ppm, $T = 1313$ K, $p = 1.2$ bar; $x_{(\text{allyl iodide})} = 4.8$ ppm, $T = 1245$ K, $p = 1.3$ bar; $x_{(\text{allyl iodide})} = 4.8$ ppm, $T = 1158$ K, $p = 1.2$ bar. The solid lines represent the results of a detailed modeling using the mechanism and rate constants given in Table 3.

In Figure 7 we present a sensitivity analysis for one experimental condition (sensitivity of each reaction relative to the sensitivity of reaction R1). From this sensitivity analysis it is seen that besides the allyl decomposition the reactions of H with allyl and propyne are most sensitive for the H-atom concentration under the conditions of this particular experiment. The sensitivity analysis also shows that at early times competing reactions are only of minor importance and, thus, justifies the approach used to determine the rate constant for the allyl dissociation.

Note that the rate constant for reaction R10 extracted in this way is in good agreement with the one predicted in ref 17 and it is, thus, in agreement with theory. Additionally, it is in fairly nice agreement (deviation of ~50%) with the one suggested by Warnatz and co-workers roughly 20 years ago.[19] Apparently, the authors of ref 19 extrapolated the rate constant from low-temperature experiments performed by Wagner and Zellner[20] as well as Whythock et al.[21] Our extracted rate constant is,

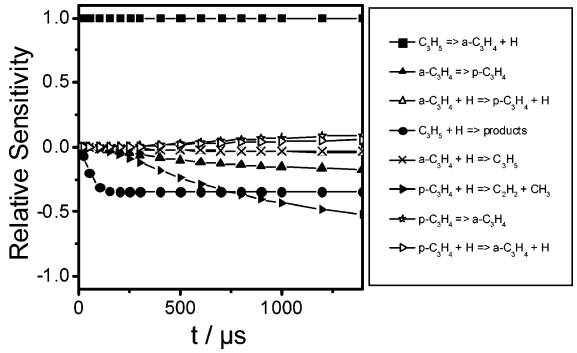

Figure 7. Sensitivity analysis for the modeled H-atom concentration−time profile. Conditions: $x_{(allyl)}$ 4.8 ppm, $T = 1477$ K, $p = 1.2$ bar.

however, up to a factor 3 greater than the one extracted by Hidaka et al. in a shock tube study on the pyrolysis of allene and propyne.[22] It is important to note that Davis et al.,[8] who modeled the propyne pyrolysis in a flow reactor, conclude that their theoretical results show that the rate coefficient for the reverse reaction ($CH_3 + C_2H_2$) is as well a factor of 3 higher than the one given by Hidaka et al.[22] Consequently, the theoretical prediction from Davis et al. is a further support for our result. We estimate the uncertainty of the rate coefficient given for R10 to be less than a factor of 2 in the temperature range of our experiments. As a result of its potential importance in combustion processes—reaction R10 and its backward reaction might act as a switch from the C3 route (propargyl recombination) and the C2 route (vinyl radical reactions) for the formation of the first aromatic ring (see also ref 23)—further studies on this reaction seem to be desirable, and we are currently investigating R10 in our laboratory.

Conclusion

The thermal unimolecular decomposition of allyl radicals has been investigated directly for the first time. The rate constant was found to be pressure-dependent, and the experimentally observed pressure dependence could be reproduced with a master equation analysis. On the basis of the results of our master equation and RRKM computations we conclude that allyl dissociates predominantly under formation of H and allene and that the competing reactions (R2 and R3) are of negligible importance. Additionally, the RRKM calculations for the specific rate constants indicate that specific rate constants from the literature might be wrong or rather wrongly assigned. Finally, the experimentally observed H-atom concentration-time profiles allowed for an extraction of the rate constant for the H + propyne reaction under high-temperature conditions. The rate constant extracted in this way is in good agreement with recent theoretical predictions.[8,22]

Acknowledgment. Financial support by the Deutsche Forschungsgemeinschaft (SFB 551, Kohlenstoff aus der Gasphase: Elementarreaktionen, Strukturen, Werkstoffe) is gratefully acknowledged. We also thank Melanie Klinger for assistance with some of the experiments during her practical lab course.

Appendix

The following are the molecular parameters used for RRKM calculation and the master equation analysis.

$CH_2CHCH_2 \rightarrow CH_2CCH_2 + H$	*(R1)*
allyl radical	
vibrational frequencies (cm^{-1})	ν = 3161, 3158, 3065, 3059, 3055, 1471, 1469, 1377, 1235, 1177, 1009, 983, 905, 788, 769, 537, 515, 412 (ref 8)
rotational constants (cm^{-1})	$A = 1.8358$; $B = 0.317$; $C = 0.2905$ (ref 8)
Lennard-Jones parameter	$\sigma = 4.85 \times 10^{-10}$ m; $\epsilon/k_B = 260$ K (ref 8)
threshold energy (R1)	20 984 cm^{-1} (ref 8)
reaction degeneracy	$L^* = 2$
prolate symm. top	
transition state	
vibrational frequencies (cm^{-1})	ν = 3141, 3129, 3053, 3047, 1939, 1426, 1375, 1062, 984, 978, 857, 825, 822, 486, 431, 375, 140 (ref 8)
	722i, imaginary frequency (ref 8)
rotational constants (cm^{-1})	$A = 2.123$; $B = 0.287$; $C = 0.287$ (ref 8)
$CH_2CHCH_2 \rightarrow CH_3CCH_2$	*(R2)*
threshold energy	22 313 cm^{-1} (ref 8)
transition state	
vibrational frequencies (cm^{-1})	ν = 3113, 3109, 2995, 2981, 2146, 1645, 1405, 1377, 1109, 1066, 990, 946, 811, 808, 676, 394, 297 (ref 8)
	1864i, imaginary frequency (ref 8)
rotational constants (cm^{-1})	$A = 2.575$; $B = 0.289$; $C = 0.289$ (ref 8)
reaction degeneracy	$L^* = 4$
$CH_2CHCH_2 \rightarrow CH_3CHCH$	*(R3)*
threshold energy	22 383 cm^{-1} (ref 8)
transition state	
vibrational frequencies (cm^{-1})	ν = 3107, 3083, 3056, 2988, 1806, 1600, 1379, 1194, 1096, 1024, 1019, 914, 893, 870, 670, 617, 444 (ref 8)
	2092i, imaginary frequency (ref 8)
rotational constants (cm^{-1})	$A = 1.286$; $B = 0.381$; $C = 0.381$ (ref 8)
reaction degeneracy	$L^* = 2$
argon	
Lennard-Jones parameter	$\sigma = 3.47 \times 10^{-10}$ m; $\epsilon/k_B = 114$ K (ref 24)

References and Notes

(1) Pope, C. J.; Miller, J. A. *Proc. Combust. Inst.* **2000**, *28*, 1519.
(2) Tsang, W.; Walker, J. A. *J. Phys. Chem.* **1992**, *96*, 8378.
(3) Deyerl, H.-J.; Fischer, I.; Chen, P. *J. Chem. Phys.* **1999**, *110*, 1450.
(4) Eng, R. A.; Gebert, A.; Hippler, H. *Proc. Combust. Inst.* **2000**, *28*, 1537.
(5) Apple, D.; Appleton, J. P. *Proc. Combust. Inst.* **1975**, *15*, 701.
(6) Just, Th. In *Shock Waves in Chemistry*; Lifshitz, A., Ed.; M. Decker: New York, 1981.
(7) Eng, R. A.; Gebert, A.; Goos, E.; Hippler, H.; Kachiani, C. *Phys. Chem. Chem. Phys.* **2001**, *3*, 2258.
(8) Davis, S. C.; Law, C. K.; Wang, H. *J. Phys. Chem. A* **1999**, *103*, 5889.
(9) Hanning-Lee, M. A.; Green, N. J. B.; Pilling, M. J.; Robertson, S. H. *J. Phys. Chem.* **1993**, *97* (7), 860.
(10) Feng, Y.; Niiranen, J. T.; Bencsura, A.; Knyazev, V. D.; Gutman, D.; Tsang, W. *J. Phys. Chem.* **1993**, *97*, 871.
(11) Gilbert, T.; Grebner, T. L.; Fischer, I.; Chen, P. *J. Chem. Phys.* **1999**, *110*, 5485.
(12) Zierhut, N.; Roth, W.; Fischer, I. *J. Phys. Chem. A* **2004**, *108*, 8125.
(13) Frost, W. *Unimolecular Reactions*; Cambridge University Press: Cambridge, 2000.
(14) Miller, J. A.; Klippenstein, S. J. *Phys. Chem. Chem. Phys.* **2004**, *5*, 1192.
(15) Isemer, S. J.; Luther, K.; Troe, J. Private communication.
(16) Harding, L. B.; Klippenstein, S. J. *Proc. Combust. Inst.* **2000**, *28*, 1503.
(17) Wang, B.; Hou, H.; Gu, Y. *J. Chem. Phys.* **2000**, *112*, 8458.

(18) Fernandes, R. X. PhD Thesis, University of Karlsruhe, Karlsruhe, Germany, 2003.
(19) Warnatz, J.; Bockhorn, H.; Möser, A.; Wenz, H. W. *Proc. Combust. Inst.* **1982**, *19*, 197.
(20) Wagner, H. Gg.; Zellner, R. *Ber. Bunsen-Ges. Phys. Chem.* **1972**, *76*, 518.
(21) Whytock, D. A.; Payne, W. A.; Stief, L. J. *J. Chem. Phys.* **1976**, *65*, 191.
(22) Hidaka, Y.; Nakamura, T.; Miyauchi, A.; Shiraishi, T.; Kawano, H. *Int. J. Chem. Kinet.* **1989**, *21*, 643.
(23) Kislitsyn, M. N.; Slagle, I. R.; Knyazev, V. D. *Proc. Combust. Inst.* **2002**, *29*, 1237.
(24) Mourits, F. M.; Rummers, F. H. A. *Can. J. Chem.* **1977**, *55*, 3007.
(25) Rohrig, M.; Petersen, E. L.; Davidson, D. F.; Hanson, R. K. *Int. J. Chem. Kinet.* **1996**, *28*, 599.
(26) Baulch, D. L.; Cobos, C. J.; Cox, R. A.; Esser, C.; Frank, P.; Just, Th.; Kerr, J. A.; Pilling, M. J.; Troe, J.; Walker, R. W.; Warnatz, J. Evaluated kinetic data for combustion modelling. *J. Phys. Chem. Ref. Data* **1992**, *21*, 411.
(27) Bozzelli, J. W.; Chang, A.; Dean, A. M. *Proc. Combust. Inst.* **1994**, *25*, 965.
(28) Tsang, W.; Herron, J. T. *J. Phys. Chem. Ref. Data* **1991**, *20*, 609.
(29) Warnatz, J. Rate coefficients in the C/H/O System. In *Combustion Chemistry*; Gardiner, W. C., Jr., Ed.; Springer: New York, 1984.
(30) Ernst, J.; Wagner, H. Gg.; Zellner, R. *Ber. Bunsen-Ges. Phys. Chem.* **1977**, *81*, 1270.
(31) Cohen, N.; Westberg, K. R. *J. Phys. Chem. Ref. Data* **1983**, *12*, 531.
(32) Miller, J. A.; Klippenstein, S. J. *J. Phys. Chem. A* **2003**, *107*, 2680.